Kirchhoff-approximate inversion of teleseismic wavefields

M. G. Bostock

Department of Earth and Ocean Sciences, The University of British Columbia, Vancouver BC, V6T 1Z4, *Canada. E-mail: bostock@geop.ubc.ca*

SUMMARY
We derive Kirchhoff-approximate inversion formulae for elastic wavefields that recover the location of discontinuity surfaces and associated material property contrasts in laterally varying, stratified media. The derivation is cast in the context of teleseismic wavefield scattering in a 2-D medium with allowance made for oblique incidence, although a fully general derivation for 3-D media follows in straightforward fashion. We exploit a little-used variant of the isotropic, elastic Kirchhoff-Helmholtz integral in which individual terms are directly identified with scattered *P*- and *S*-wave contributions *prior* to approximation using ray-theoretic forms. This approach yields relatively simple formulae for Kirchhoff-approximate forward modelling that bear a closer resemblance to their acoustic counterpart than standard elastic formulations cast in terms of traction and displacement. Using micro-local analysis, inversion formulae are readily derived using the generalized Radon transform. Our approach represents an extension of the Kirchhoff-approximate inversion scheme outlined by Beylkin & Burridge (1990) to *S*-waves and conversions. We demonstrate application of the method to field data recorded during the IRIS-PASSCAL CASC93 experiment.

Key words: body waves, inversion, mantle discontinuities, scattering.

1 INTRODUCTION

Multichannel processing of scattered teleseismic body waves has become a topic of considerable interest in recent years owing to the increased availability of large numbers of multicomponent seismometers (e.g. Dueker & Sheehan 1997; Revenaugh 1995; Ryberg & Weber 2000; Shearer *et al.* 1999). A majority of these studies has drawn heavily on a strong analogy with reflection seismology. In particular, the near-vertical propagation paths represented in both instances, together with a dominantly vertical variation in Earth's material properties, allow the assumption of single scattering to be made in imaging (migration) and inversion (migration and material property estimation).

There are two different integral formulations of the wave equation that are often adopted as the starting point for migration/inversion in reflection seismology. Scattering from localized volume heterogeneity is most readily treated using the so-called Born approximation, the linearization of an exact integral equation of Lippman-Schwinger type. Recently, a (high-frequency) asymptotic method based on the Born approximation and accommodating realistic receiver-array geometries and source distributions, has been adapted for inverting scattered teleseismic waveforms recorded on dense linear arrays of three-component seismometers (Bostock *et al.* 2001). The method relies on the identification of the inverse scattering problem with a generalized Radon transform (Beylkin 1985; Miller *et al.* 1987; Beylkin & Burridge 1990), and effectively recovers a high-pass filtered version of the perturbations in material parameters defined with respect to some smoothly varying reference medium.

The viability of this approach has been demonstrated through its application to field data recorded over the Cascadia subduction zone (Rondenay *et al.* 2001).

In many circumstances, however, the structures of interest may be better characterized by laterally variable stratification than by localized heterogeneity, as, for example, in typical applications of the widely used receiver-function technique (Langston 1979; Vinnik 1977). This latter observation serves as motivation for the current study where we examine the application to teleseismic data sets of a second, widely used integral formulation of inverse scattering: the Kirchhoff-Helmholtz integral. Through its representation of the wavefield as a surface integral, this formulation and its asymptotic implementation, the Kirchhoff approximation, afford a description of scattering from laterally variable but dominantly stratified media that may be a useful alternative to the Born approximation in some environments.

In this paper, we derive the Kirchhoff-Helmholtz integral for an acquisition geometry corresponding to typical teleseismic experiments. Specifically, this geometry involves the oblique incidence of a plane wave upon a non-planar interface separating two slowly varying, two-dimensional (2-D) media. Although formally equivalent to more widely employed versions of the Kirchhoff-Helmholtz integral cast in terms of traction and displacement (e.g. Kuo & Dai 1984; Frazer & Sen 1985; Sumner 1987), the variant we adopt (Morse & Feshbach 1953; Waterman 1978) permits a more direct identification of individual wave modes as specified in the Kirchhoff approximation. We are thereby able to identify relatively simple forms for the elastic Kirchhoff approximation corresponding directly to *P*- and

S-waves, that bear a closer resemblance to their extensively cited acoustic counterpart. Using micro-local analysis, approximate inverse formulae for material property contrasts across singular functions of discontinuities (Bleistein 1987; Beylkin & Burridge 1990) can be derived, once more, in terms of generalized Radon transforms. By including *S*-waves and conversions, our study extends the approach of Beylkin & Burridge (1990) (who outlined a Kirchhoff-approximate inversion formalism for *P*-to-*P* reflections) to general isotropic, elastic scattering. We demonstrate application of of this approach to synthetic and field data sets.

2 THE 2-D KIRCHHOFF-HELMHOLTZ INTEGRAL FOR OBLIQUE INCIDENCE

Consider the situation depicted in Fig. 1. An irregular boundary, S_B, with strike parallel to coordinate x_2 separates two smoothly varying, 2-D elastic half-spaces. For the present, we shall focus our attention upon an upgoing wavefield $U_i^0(\mathbf{x})$ of, yet, unspecified type (i.e. compressional or shear) incident upon S_B from below. In anticipation of the teleseismic application, we will require this wavefield to be approximately planar, and, in particular, that it be accurately characterized by a harmonic dependence on the x_2 coordinate as $U_i^0(\mathbf{x}) = u_i^0(x_1, x_3)e^{i\omega p_2 x_2}$, where ω is radial frequency and p_2 is the component of phase slowness in the x_2 direction. The interaction of this wavefield with the boundary S_B produces a reflected wave propagating downward into medium 2 (with which we shall be concerned no further) and a transmitted wave that propagates upward into medium 1. The displacement wavefield in the upper medium $U_i(\mathbf{x}) = u_i(x_1, x_3)e^{i\omega p_2 x_2}$ retains the harmonic dependence in x_2 by virtue of the inherent two dimensionality, and satisfies

$$L_{ik}U_k = \partial_j\left(c_{ijkl}^{(1)}\partial_l U_k\right) + \rho_1\omega^2 U_i = 0, \tag{1}$$

where $c_{ijkl}^{(1)} = c_{ijkl}^{(1)}(x_1, x_3)$ and $\rho_1 = \rho_1(x_1, x_3)$ are the elastic tensor and density, respectively, in the upper medium. To proceed we must
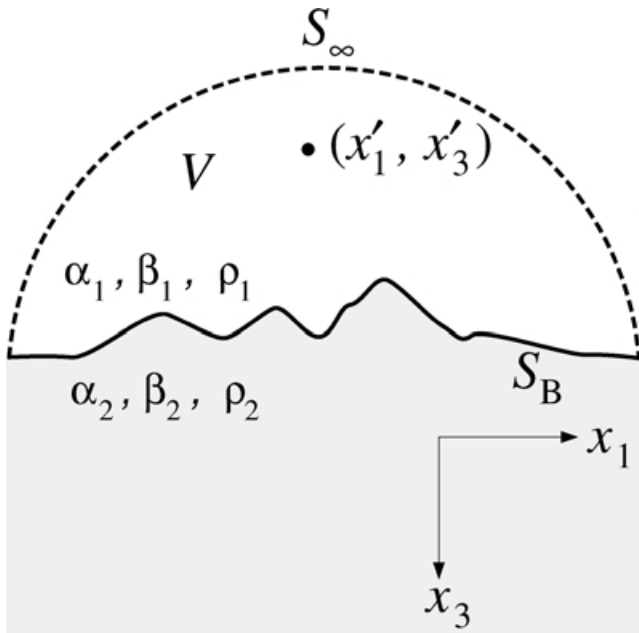

Figure 1. Model geometry for derivation of 2-D Kirchhoff modelling formulae. A laterally variable boundary S_B separates two slowly varying, isotropic media characterized by velocities and density $\alpha_1, \beta_1, \rho_1$ and $\alpha_2, \beta_2, \rho_2$. The volume V is enclosed by a surface defined by the union of interface S_B and a semi-circular surface S_∞.

introduce the adjoint operator $L_{ik}^\dagger$ and its associated Green's function $G_{in}^\dagger(\mathbf{x}, \mathbf{x}') = g_{in}^\dagger(x_1, x_3; x_1'x_3')e^{-i\omega p_2 x_2}$ (see Bostock *et al.* 2001) for the upper medium that, together, satisfy

$$L_{ik}^\dagger G_{kn}^\dagger = -\delta_{in}\delta(x_1 - x_1')\delta(x_3 - x_3')e^{-i\omega p_2 x_2}. \tag{2}$$

We now contract (1) with $G_{in}^\dagger(\mathbf{x}, \mathbf{x}')$ and (2) with $U_i(\mathbf{x})$, subtract, and integrate through a semi-cylindrical volume V as depicted in Fig. 1. By employing the divergence theorem, and noting that the resulting integral is independent of x_2, we are able to recast the volume integral as a 2-D surface integral

$$u_n(x_1', x_3') = \int_S dS n_j c_{ijkl}^{(1)}\left[\partial_l U_k(\mathbf{x})G_{in}^\dagger(\mathbf{x}, \mathbf{x}') - \partial_l G_{kn}^\dagger(\mathbf{x}, \mathbf{x}')U_i(\mathbf{x})\right], \tag{3}$$

confined to the (x_1, x_3) plane (we have specified the general dependence on $\mathbf{x}$, $\mathbf{x}'$ within the integrand to allow a compact indicial expression in terms of the operator ∂_2). The surface S is defined by an outward normal n_j lying within the (x_1, x_3) plane and consists of 2 parts: a semi-circular cap S_∞ and that portion of the boundary S_B which underlies it. Eq. (3) is one form of the Kirchhoff-Helmholtz integral (Pao & Varatharajulu 1976) tailored to the 2-D, oblique incidence geometry we have specified.

We will henceforth restrict our attention to isotropic media, for which the elastic tensor of the upper medium is written as

$$c_{ijkl}^{(1)} = \lambda_1\delta_{ij}\delta_{kl} + \mu_1(\delta_{il}\delta_{jk} + \delta_{ik}\delta_{jl}), \tag{4}$$

where $\lambda_1 = \lambda_1(x_1, x_3)$, $\mu_1 = \mu_1(x_1, x_3)$ are the Lamé parameters. In most seismological applications, the Kirchhoff approximation is made at this point to avoid having to solve a Fredholm equation. More specifically, the Kirchhoff approximation involves adopting high frequency (i.e. ray-theoretic) approximations for the (displacement and traction) wavefields and replacing $U_i(x_1, x_3)$ in (3) by the product of the incident wave-amplitude in the lower medium and the local plane-wave transmission coefficient at (x_1, x_3). We shall, however, postpone this step and follow Pao & Varatharajulu (1976) by subtracting the null quantity

$$\int_V dV \mu_1 \nabla \cdot \left[\nabla \times \left(\mathbf{U} \times \mathbf{G}_n^\dagger\right)\right] = 0$$

$$= \int_S dS \mu_1 \mathbf{n} \cdot \left[\nabla \times \left(\mathbf{U} \times \mathbf{G}_n^\dagger\right)\right] \tag{5}$$

from (3). In this and ensuing developments, it will prove convenient to express quantities in a more compact vector notation, and we define, for example, $\mathbf{G}_n^\dagger(\mathbf{x}, \mathbf{x}')$ to be the *n*th column of the 2nd rank tensor $G_{in}^\dagger(\mathbf{x}, \mathbf{x}')$. Using elementary vector identities it is easy to show that (3) can then be recast as

$$u_n(x_1', x_3') = \int_S dS(\lambda_1 + 2\mu_1)\left[(\mathbf{n} \cdot \mathbf{G}_n^\dagger)(\nabla \cdot \mathbf{U}) - (\mathbf{n} \cdot \mathbf{U})(\nabla \cdot \mathbf{G}_n^\dagger)\right]$$
$$+ \mu_1\left[(\mathbf{n} \times \mathbf{G}_n^\dagger) \cdot (\nabla \times \mathbf{U}) - (\mathbf{n} \times \mathbf{U}) \cdot (\nabla \times \mathbf{G}_n^\dagger)\right]. \tag{6}$$

We emphasize that this equation is valid for variable λ_1, μ_1 and is similar to eq. (13.1.40) of Morse & Feshbach (1953), although more symmetric in form and without the volume source term. As such, it represents a variant of the Kirchhoff-Helmholtz integral that has, apparently, received scant attention in seismology. The dot product in (5) represents a solenoidal contribution that integrates to zero over a closed surface and can be associated with the near-field (Waterman 1978). Eq. (6) holds the advantage that (curl-free)

P-wave and (divergence-free) *S*-wave contributions are immediately evident and isolated within the individual terms. This is clearly useful in circumstances where the surface boundary conditions are specified in terms of wave modes (vs traction and displacement), as for example, in the Kirchhoff approximation.

To complete the derivation, we extend the radius of the surface S_∞ out to infinity where we note that the individual *P*- and *S*-wave components of **U** and $\mathbf{G}_n^\dagger$ are outgoing (assuming that scattering within the slowly varying 2-D medium is negligible) such that this portion of the surface integral vanishes by virtue of the Sommerfeld radiation condition. Thus we may restrict integration in (6) to the boundary S_B alone. Note, moreover, that the derivation outlined above may be repeated for an incident wavefield impinging on S_B from above, in which case $\mathbf{U}(\mathbf{x})$ in (6) is taken to be the resulting, upward propagating, backscattered wavefield.

3 THE KIRCHHOFF APPROXIMATION

Eq. (6) represents the displacement at some point (x_1', x_3') interior to the upper medium in terms involving the curl and divergence of both the wavefield and the Green's function of the upper medium evaluated at the interface S_B. As mentioned above, we may further associate the individual terms with scattered *P*- and *S*-waves. To apply the Kirchhoff approximation, we write the Green's function in a high-frequency asymptotic form that identifies both *P*- and *S*-wave contributions as

$$G_{in}^\dagger(\mathbf{x},\mathbf{x}') = \hat{A}^P(\mathbf{x},\mathbf{x}')\mathrm{e}^{\mathrm{i}\omega\hat{\tau}^P(\mathbf{x},\mathbf{x}')}\hat{s}_i^P(\mathbf{x})\hat{s}_n^P(\mathbf{x}') + \hat{A}^S(\mathbf{x},\mathbf{x}')\mathrm{e}^{\mathrm{i}\omega\hat{\tau}^S(\mathbf{x},\mathbf{x}')}$$
$$\times\left[\hat{s}_i^v(\mathbf{x})\hat{s}_n^v(\mathbf{x}') + \hat{s}_i^h(\mathbf{x})\hat{s}_n^h(\mathbf{x}')\right] \quad (7)$$

where $\hat{A}^P$, $\hat{A}^S$ incorporate geometrical spreading amplitudes, $\hat{\tau}^P$, $\hat{\tau}^S$ are traveltimes and $\hat{s}_i^P$, $\hat{s}_i^v$, $\hat{s}_i^h$ are polarization vectors (superscripts v, h identify two mutually orthogonal *S*-polarization vectors, and need not be tied to the specific coordinate directions). In like fashion, we express the scattered wavefield within the upper medium as

$$U_i(\mathbf{x}) = \check{A}^P(\mathbf{x})\mathrm{e}^{\mathrm{i}\omega\check{\tau}^P(\mathbf{x})}\check{s}_i^P(\mathbf{x}) + \check{A}^S(\mathbf{x})\mathrm{e}^{\mathrm{i}\omega\check{\tau}^S(\mathbf{x})}\check{s}_i^S(\mathbf{x}), \quad (8)$$

and the incident wavefield as

$$U_i^0(\mathbf{x}) = \tilde{A}^P(\mathbf{x})\mathrm{e}^{\mathrm{i}\omega\tilde{\tau}^P(\mathbf{x})}\tilde{s}_i^P(\mathbf{x}) + \tilde{A}^S(\mathbf{x})\mathrm{e}^{\mathrm{i}\omega\tilde{\tau}^S(\mathbf{x})}\tilde{s}_i^S(\mathbf{x}). \quad (9)$$

Note that accents ˆ, ˇ, ˜ identify quantities associated with the Green's function, scattered wavefield and incident wavefield, respectively. The polarization directions of *P*-waves will be taken to be parallel to and positive in the direction of propagation. For scattered *S*-waves it will prove convenient to decompose the polarization vector $\check{s}_i^S$ in terms of its components in the sagittal plane and transverse direction as defined by the local geometry of the incident and scattered rays at S_B. Accordingly, we define corresponding unit polarization vectors as

$$\check{\mathbf{s}}^V = -\frac{\nabla\check{\tau}^S \times (\nabla\check{\tau}^S \times \nabla\tilde{\tau})}{|\nabla\check{\tau}^S \times (\nabla\check{\tau}^S \times \nabla\tilde{\tau})|}, \quad \check{\mathbf{s}}^H = -\frac{\nabla\check{\tau}^S \times \nabla\tilde{\tau}^S}{|\nabla\check{\tau}^S \times \nabla\tilde{\tau}^S|}. \quad (10)$$

In (10) and what follows, we omit superscripts *P*, *S* when expressing properties of generic incident, scattered or Green's function wavefields. The *S*-polarizations, so-defined, ensure that the corresponding *S*-waves generated through reflections and conversions (assuming that $\beta_1 < \alpha_2$) comply locally (i.e. within the reference frame defined by the local normal to S_B and the plane of propagation) with the polarization convention used by Aki & Richards (1980) to define reflection and transmission coefficients (we shall implicitly assume that the incident wave also adheres to this standard).

Employing expressions (7) and (8) in (6) and retaining only those terms of highest order in frequency yields

$$\mathbf{u}(x_1', x_3') = \mathrm{i}\omega\hat{\mathbf{s}}^P(x_1', x_3')\int_{S_B} dS\rho_1\alpha_1^2\hat{A}^P\check{A}^P\mathrm{e}^{\mathrm{i}\omega(\hat{\tau}^P+\check{\tau}^P)}\mathbf{n}$$
$$\cdot(\nabla\hat{\tau}^P - \nabla\check{\tau}^P)$$
$$= \mathrm{i}\omega\hat{\mathbf{s}}^P(x_1', x_3')\int_{S_B} dS\rho_1\alpha_1^2\hat{A}^P C\tilde{A}\mathrm{e}^{\mathrm{i}\omega(\hat{\tau}^P+\tilde{\tau})}\mathbf{n}$$
$$\cdot(\nabla\hat{\tau}^P - \nabla\check{\tau}^P). \quad (11)$$

for a scattering interaction producing upward propagating *P*-waves, Here, we have substituted the arrival time of the incident wave on the boundary S_B for that of the scattered wave (where the two are equal), and the amplitude of the scattered wave has been approximated by the product of the incident wave amplitude $\tilde{A}$ and the relevant scattering coefficient C. This latter quantity will assume the value of one of the reflection/transmission coefficients R_D^{PP}, R_D^{PS}, T_U^{PP}, or T_U^{PS} depending on the propagation direction, polarization and mode-type of the incident wavefield (where, e.g. R_D^{PS} is the reflection coefficient for a downward incident *SV*-wave converted into a *P*-wave).

The corresponding equation for *S*-waves may be written

$$\mathbf{u}(x_1', x_3') = \mathrm{i}\omega\int_{S_B} dS\rho_1\beta_1^2\hat{A}^S C\tilde{A}\mathrm{e}^{\mathrm{i}\omega(\hat{\tau}^S+\tilde{\tau})}\left\{\mathbf{n}\cdot[\hat{\mathbf{s}}^v \times (\nabla\check{\tau}^S \times \check{\mathbf{s}}^S)\right.$$
$$-\check{\mathbf{s}}^S \times (\nabla\hat{\tau}^S \times \hat{\mathbf{s}}^v)]\hat{s}^v(x_1', x_3') + \mathbf{n}\cdot[\hat{\mathbf{s}}^h \times (\nabla\check{\tau}^S \times \check{\mathbf{s}}^S)$$
$$\left.-\check{\mathbf{s}}^S \times (\nabla\hat{\tau}^S \times \hat{\mathbf{s}}^h)]\hat{s}^h(x_1', x_3')\right\}, \quad (12)$$

where we must now allow for independent *S*-wave interactions in the sagittal plane and transverse direction; thus *C* can assume values of R_D^{VV}, R_D^{SP}, R_D^{HH}, T_U^{VV}, T_U^{SP}, or T_U^{HH} depending, again, on the local nature of the incident wavefield. For strictly 2-D, in-plane propagation (i.e. $p_2 = 0$) the two *S*-wave polarizations are decoupled, and the sum of dot products in (12) reduces to an individual term with a form similar to that in (11) for *P*-waves, that is, involving $\mathbf{n}\cdot(\nabla\hat{\tau}^S - \nabla\check{\tau}^S)$. Eqs (11) and (12) (or their 3-D analogues) can be used for forward modelling to the same order of accuracy as those previously derived by, e.g. Kuo & Dai (1984), Frazer & Sen (1985) and Sumner (1987).

4 INVERSION VIA GENERALIZED RADON TRANSFORM

Our goal in this section is to cast the integrals in (11) and (12) into forms that will allow us to derive direct inversion formulae using the generalized Radon transform (Beylkin 1985; Miller *et al.* 1987; Beylkin & Burridge 1990). We note, however, that both integrals contain factors that depend directly on **n**, that is, they require *a priori* knowledge of the scattering surface geometry. This requirement may be removed by using the so-called microlocalization technique (Beylkin & Burridge 1990) that allows us to replace **n** by its value at the specular point and to set $\nabla\check{\tau} = -\nabla\hat{\tau}$ (in effect, this simply acknowledges that we are interested in reconstruction of quasi-planar discontinuities). In particular, for top-side reflections and upward *P*-to-*S* transmission-conversions (assuming, once more, that $\beta_1 < \alpha_2$), we have

$$\mathbf{n} = \frac{\nabla\hat{\tau} + \nabla\tilde{\tau}}{|\nabla\hat{\tau} + \nabla\tilde{\tau}|}, \quad (13)$$

a relation easily derived upon application of Snell's law. For upward *S*-to-*P* transmission-conversions we must negate this quantity, whereas the sign will depend on the polarity of the velocity contrast

Table 1. Scattering mode related quantities.

Scattering mode m	Scattering coefficient C^m	Incident velocity $\tilde{c}$	Scattered velocity $\hat{c}$	Polarization factor S_n^m
1	R_D^{PP}	α_1	α_1	$\hat{s}_n^P$
2	R_D^{PS}	β_1	α_1	$\hat{s}_n^P$
3	R_D^{VV}	β_1	β_1	$-\beta_1\left[\hat{s}_n^v(\hat{\mathbf{s}}^v \cdot \nabla\tilde{\tau}^S) + \hat{s}_n^h(\hat{\mathbf{s}}^h \cdot \nabla\tilde{\tau}^S)\right]\big/\sin\theta$
4	R_D^{SP}	α_1	β_1	$-\alpha_1\left[\hat{s}_n^v(\hat{\mathbf{s}}^v \cdot \nabla\tilde{\tau}^P) + \hat{s}_n^h(\hat{\mathbf{s}}^h \cdot \nabla\tilde{\tau}^P)\right]\big/\sin\theta$
5	R_D^{HH}	β_1	β_1	$\beta_1^2\left[\hat{s}_n^v(\hat{\mathbf{s}}^v \cdot \nabla\tilde{\tau}^S \times \nabla\hat{\tau}^S) + \hat{s}_n^h(\hat{\mathbf{s}}^h \cdot \nabla\tilde{\tau}^S \times \nabla\hat{\tau}^S)\right]\big/\sin\theta$
6	T_U^{PS}	β_2	α_1	$-\hat{s}_n^P$
7	T_U^{SP}	α_2	β_1	$-\alpha_2\left[\hat{s}_n^v(\hat{\mathbf{s}}^v \cdot \nabla\tilde{\tau}^P) + \hat{s}_n^h(\hat{\mathbf{s}}^h \cdot \nabla\tilde{\tau}^P)\right]\big/\sin\theta$

across the interface for intramode transmissions. We will henceforth exclude intramode transmissions from our analysis as their relative insensitivity to structure and difficulties in effective pre-processing render them practically useless for imaging purposes in the present context (e.g. Shragge *et al.* 2001).

Substitution of (13) into (11) and (12) using the relation (10) enables us, after some algebra, to write the scattering integrals in a compact form as

$$u_n^m(x_1', x_3') = -\sqrt{-i\omega} \int_{S_B} dS\, C^m(\theta)\mathcal{A}_n^m e^{i\omega\mathcal{T}^m}, \qquad (14)$$

where we have extracted the frequency dependence $1/\sqrt{-i\omega}$ from the amplitudes $\hat{A}$ of the 2-D Green's function (see e.g. Bostock *et al.* 2001, Appendix A). The index m identifies the scattering mode interaction as defined in Table 1, whereas $\mathcal{T}^m$ and $\mathcal{A}_n^m$ represent compound traveltime and amplitude quantities defined by

$$\mathcal{T}^m = \tilde{\tau} + \hat{\tau}. \qquad (15)$$

and

$$\mathcal{A}_n^m = 2\sqrt{-i\omega}\rho_1\hat{c}^2 \tilde{A}\hat{A}\frac{\nabla\hat{\tau} \cdot \nabla\mathcal{T}^m}{|\nabla\mathcal{T}^m|} S_n^m(\mathbf{x}, \mathbf{x}'), \qquad (16)$$

Note that $\tilde{A}$, $\tilde{\tau}$ and $\hat{A}$, $\hat{\tau}$ are the amplitude and traveltime of incident wave and Green's function, respectively, corresponding to mode interaction m. The relevant reflection/transmission coefficient is now identified by $C^m(\theta)$ where θ is the so-called scattering angle between the incident and Green's function rays (see Fig. 2), i.e.

$$\cos\theta = \tilde{c}\hat{c}\nabla\tilde{\tau} \cdot \nabla\hat{\tau}. \qquad (17)$$

The velocities of the incident and scattered waves for mode-interaction m are represented by $\tilde{c}$ and $\hat{c}$, respectively, and are defined explicitly along with the polarization-dependent factors $S_n^m(\mathbf{x}, \mathbf{x}')$ in Table 1. Note that for strictly 2-D in-plane propagation (i.e. $p_2 = 0$), the polarization factors $S_n^m(\mathbf{x}, \mathbf{x}')$ involving S-waves reduce to single terms analogous to those for P-waves.

Before proceeding, we observe that evaluation (16) will, for transmitted conversions, require a knowledge of material velocities both above and below the interface S_B. For reflected waves the requirement is less stringent and only velocities above the reflector are needed. Thus, whereas it is possible to contemplate inversion schemes involving reflected waves in which one might iteratively bootstrap the model solution (including both interface locations and layer velocities) in depth (Bleistein 1987), it would appear that transmitted waves alone could afford the location of interfaces only once layer velocities are known. From a practical point of view, however, velocities will not be known exactly either above or below an interface; rather, we will have, at best, an accurate *a priori* appreciation of

the slowly varying component of velocity structure. Consequently, we shall take the view that we know this slowly varying component, and adopt a small contrast, perturbative approximation for short-wavelength structure. Accordingly, we shall replace the exact velocities across the interface in (16) and Table 1 with corresponding (slowly varying) reference values,

$$\alpha_1, \alpha_2 \to \alpha, \quad \beta_1, \beta_2 \to \beta, \quad \rho_1, \rho_2 \to \rho, \qquad (18)$$

and allow the true values to be recovered through a set of corresponding (small) perturbations, $\Delta\alpha, \Delta\beta, \Delta\rho$ as, e.g. $\alpha_1 = \alpha - \Delta\alpha/2$, $\alpha_2 = \alpha + \Delta\alpha/2$.

We proceed to introduce the singular function $d(s)$ of the surface S_B (Bleistein 1987) that allows us to recast the surface integrals in (14) as (2-D) volume integrals, that is

$$u_n^m(x_1', x_3') = -\sqrt{-i\omega} \int_V dV\, d(s)C^m\mathcal{A}_n^m e^{i\omega\mathcal{T}^m}. \qquad (19)$$

By applying a filter $F(\omega) = -\sqrt{-i\omega}\mathrm{i}\,\mathrm{sgn}(\omega)$ to $u_n^m(x_1', x_3')$, followed by inverse Fourier transformation, we define a new, time-domain quantity $v_n^m(x_1', x_3', t)$

$$v_n^m(x_1', x_3', t) = \frac{1}{2\pi} \int d\omega e^{-i\omega t} F(\omega)u_n^m(x_1', x_3')$$

$$= -\int dV\, d(s)C^m\mathcal{A}_n^m\mathcal{H}\{\delta'(t - \mathcal{T}^m)\}, \qquad (20)$$
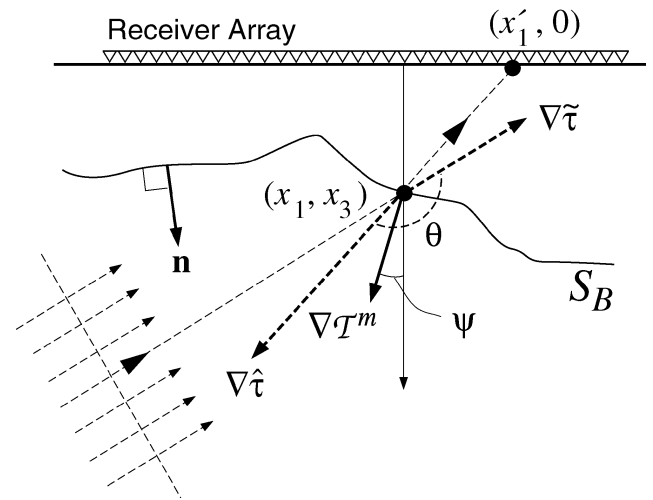

Figure 2. Geometrical variables employed in the derivation of Kirchhoff-approximate inversion formulae for 2-D structure. Note that quantities $\mathbf{n}$, $\nabla\mathcal{T}^m$ and ψ are measured within the $x_1 - x_3$ plane whereas $\nabla\hat{\tau}$, $\nabla\tilde{\tau}$ and θ, in general, possess out-of-plane components.

where $\mathcal{H}\{\cdot\}$ denotes Hilbert transform. This last integral can be identified as a 2-D inverse generalized Radon transform, (see Miller *et al.* 1987; Bostock *et al.* 2001) and approximately inverted using the corresponding forward transform as

$$\langle d(s) C^m \rangle = \frac{1}{4\pi} \int d\psi \frac{|\nabla \mathcal{T}^m|^2}{|\mathcal{A}^m|^2} \sum_n \mathcal{A}_n^m v_n^m(x_1', x_3', t = \mathcal{T}^m), \quad (21)$$

where the angle ψ is defined in Fig. 2 and $|\mathcal{A}^m|^2 = \sum_n \mathcal{A}_n^m \mathcal{A}_n^m$. The recovered quantity identifies both the location of the interface $d(s)$ and the strength of the scattering coefficient $C^m(\theta)$ for the angular sampling afforded by any particular source.

While useful for imaging structure using a single event, we may wish to advance beyond the scattering coefficient to extract estimates of the material contrasts represented by the scattering surface S_B. Several options are open to us at this point. We may choose to adopt the approach of Bleistein (1987) and introduce an additional factor within (21) allowing a specular angle for the particular scattering coefficient to be estimated. Then, using images for multiple sources, one may perform a (post-imaging) amplitude-vs-angle analysis to recover material properties. An alternative approach suggested by Beylkin & Burridge (1990) and one we shall adopt, involves linearization of the R/T coefficients (Aki & Richards 1980) in compliance with the small-contrast approximation made earlier. This approach allows us to consider multiple source-receiver combinations in a simultaneous inversion for material property perturbations, an important advantage when dealing with (often noisy and sparsely sampled) teleseismic data. Explicitly, we may write

$$C^m(\theta) = \sum_l W_l^m(\theta) \Delta m_l, \quad (22)$$

where $\Delta m_l = \Delta\alpha/\alpha, \Delta\beta/\beta, \Delta\rho/\rho$ for $l = 1, 2, 3$. The weighting coefficients $W_l^m(\theta)$ are given in the appendix in terms of the quantities defined in Fig. 2.

Following Bostock *et al.* (2001), we recast (21) as a least-squares inversion for material properties in terms of variables more directly associated with the experimental set-up, namely the (approximate) source backazimuth γ, (absolute value of) horizontal slowness $|\mathbf{p}_\perp^0|$, and receiver position x_1'. This entails the introduction of a Jacobian for the appropriate transformation of variables (Beylkin 1985) to define 3 potential functions $g_l(x_1, x_3)$ as, e.g.

$$g_l(x_1, x_3) = \frac{1}{4\pi} \int d|\mathbf{p}_\perp^0| \int d\gamma \int dx_1' \left| \frac{\partial(\psi, \theta)}{\partial(x_1', \gamma)} \right|$$
$$\times \sum_m W_l^m(\theta) \frac{|\nabla \mathcal{T}^m|^2}{|\mathcal{A}^m|^2} \sum_n \mathcal{A}_n^m v_n^m(x_1', \mathbf{p}_\perp^0, t = \mathcal{T}^m),$$
$$(23)$$

that are simply weighted diffraction stacks of the filtered data v_n^m over all sources and receivers. Several forms of the Jacobian valid for 1-D reference media and potentially useful in teleseismic applications are provided in Appendix B of Bostock *et al.* (2001). The material property perturbations at any particular image point (x_1, x_3) can be retrieved from these potentials through a trivial 3×3 matrix inversion and multiplication as

$$\Delta \mathsf{m} = (\mathsf{W}^T \mathsf{W})^{-1} \mathbf{g} = \mathsf{H}^{-1} \mathbf{g}, \quad (24)$$

where the vector $\mathbf{g}$ contains the elements g_l, matrix W contains the elements $W_l^m(\theta)$, and the elements of H are defined by

$$H_{lk}(x_1, x_3) = \int d|\mathbf{p}_\perp^0| \int d\theta \sum_m W_l^m(\theta) W_k^m(\theta). \quad (25)$$

5 GENERAL REMARKS

In the approach described above, we have considered the reconstruction of material property contrasts across a single interface separating two halfspaces in which material properties are slowly varying. By assuming that single scattering dominates such that multiple conversions/reflections are negligible (an assumption consistent with other simplifications made to this point), we can extend the Kirchhoff-approximate treatment to more complex vertical stratification involving multiple layers. In practical circumstances, of course, the presence of the free surface invalidates this assumption by creating multiples with amplitudes of the same order of magnitude as the direct wave. However, in the teleseismic situation where both the free surface and the incident wavefield can be taken to be effectively planar, we may consider the resulting free-surface (*P-* and *S-*) reflections as new sources of plane waves that illuminate structure from above to yield reflections and backscattered conversions (Bostock *et al.* 2001). Using the Kirchhoff-approximate treatment above, these reflected waves can then be treated simultaneously with the direct (i.e. forward-scattered) conversions to place further constraint on subsurface structure (Shragge *et al.* 2001; Rondenay *et al.* 2001).

Given the similarity in their derivations, it is perhaps not surprising that the Kirchhoff-approximate formalism of the present work can be implemented with rather minor modification to the Born-approximate algorithm presented by Bostock *et al.* (2001). Moreover, most of the observations made in that work concerning resolution and sensitivity of different scattering modes, also hold true here. One difference, however, is that the raw data must be pre-processed with different frequency filters; in particular, the Born-approximate data are low-pass filtered whereas the Kirchhoff-approximate data are high-pass filtered. These filters are formally required within the respective derivations to reproduce images of herogeneity as perturbations to a reference medium (Born) and as singular functions of discontinuity surfaces (Kirchhoff). The emphasis of high frequencies in the Kirchhoff technique leads to a more localized delineation of discontinuity surfaces. In addition, θ-dependent weighting factors applied to the material property perturbations in (16) and (22) differ slightly in both cases.

It should also be noted that although similar in final result, the philosophy underlying the procedure we have outlined differs in its motivation from classical Kirchhoff migration (Schneider 1978) as applied recently in seismological studies (Ryberg & Weber 2000; Shearer *et al.* 1999). The basis of the latter approach is again the Kirchhoff-Helmholtz integral, but it is employed using an acausal Green's function to back-propagate the reflected/converted wavefield to earlier times. The result is an image of the reflected/converted wavefield at its time of origin which should identify the reflector surface with a magnitude equivalent to the reflection coefficient. Our approach, in contrast, exploits the forward scattering Kirchhoff-Helmholtz integral and its analogy with the (inverse) Radon transform, in the construction of a formal inversion operator that allows estimates to be made of the contrast in material properties across a discontinuous structures. Although different in their starting points, the two approaches can be shown to yield equivalent results (Docherty 1991).

6 SYNTHETIC EXAMPLE

As a first example, we consider the inversion of pseudo-spectral synthetic seismograms generated for the simplified continental suture model of Shragge *et al.* (2001). The model consists of three
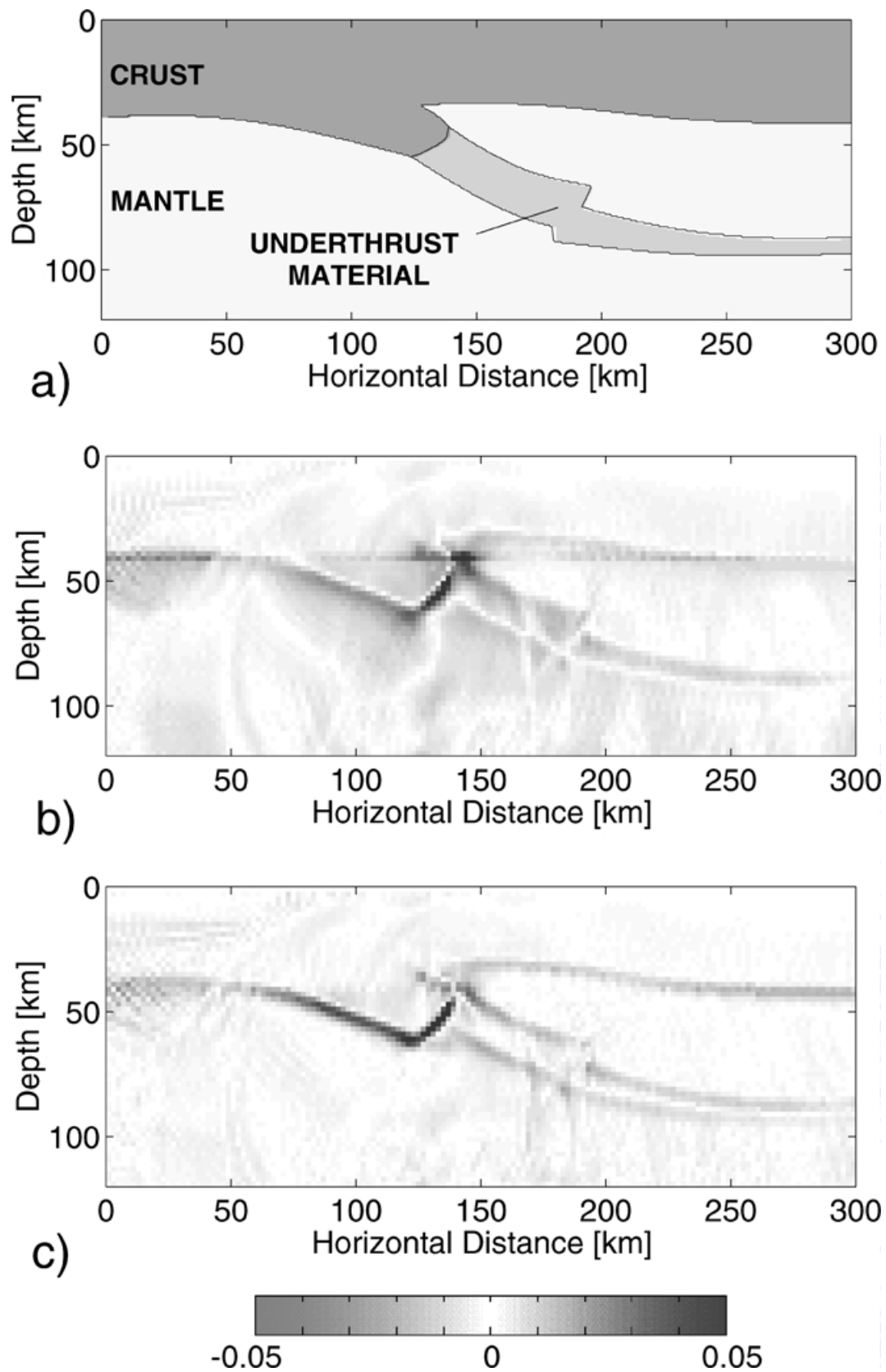
Figure 3. Results of synthetic inversion. (a) Simplistic lithospheric suture model for which pseudo-spectral synthetic seismograms were generated (see text for details). (b) Born inversion of synthetic seismograms (direct P-to-S, $m = 7$) for shear-velocity contrast $\Delta\beta/\beta$. (c) Kirchhoff inversion of same data set for $\Delta\beta/\beta$.
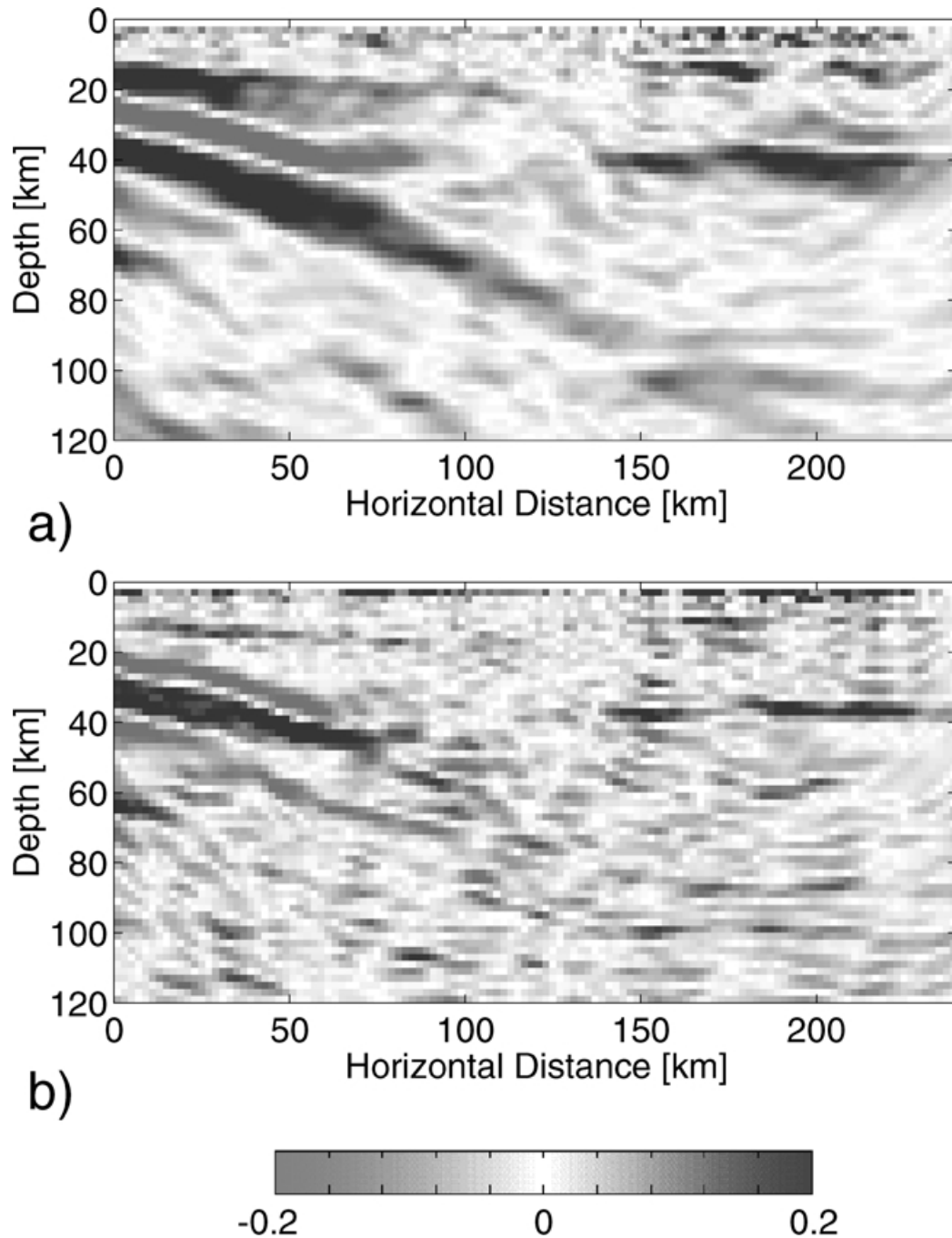
Figure 4. Results from inversion of CASC93 data. (a) Born inversion of *S*-response to free-surface *P* reflection ($m = 4$) for shear-velocity contrast $\Delta\beta/\beta$. (b) Kirchhoff inversion of same data set for $\Delta\beta/\beta$.

components: a low-velocity ($\alpha = 6.2$ km s^{-1}, $\beta = 3.6$ km s^{-1}) crust, a high-velocity ($\alpha = 8.0$ km s^{-1}, $\beta = 4.5$ km s^{-1}) mantle and under-thrust, former crustal material with still higher velocities ($\alpha = 8.1$ km s^{-1}, $\beta = 4.9$ km s^{-1}). The combination of quasi-planar boundaries and sharper corner structures present a reasonable range of complexity for the imaging algorithm. The synthetic data comprise six sets of synthetic seismograms corresponding to incident plane waves with horizontal slownesses of $\pm0.05, 0.06, 0.07$ km s^{-1}. Each of these data sets includes 120 seismograms separated at 3 km intervals and bandpass filtered between 0.03 and 2 Hz. We have inverted the data using only forward-scattered *P*-to-*S* conversions for the sake of simplicity, although a better localization of structure

could be achieved by including other scattering modes (Shragge *et al.* 2001). Moreover, we have restricted the inversion of model parameters to shear velocity contrast (i.e. $\Delta\beta/\beta$) since forward *P*-to-*S* scattering is independent, to first order, of *P*-velocity contrast and only weakly dependent upon density contrast (see e.g. A7 for $\theta \rightarrow 180°$).

The recovered structure using the Kirchhoff-approximate approach is shown along with the original structural boundaries and the Born-approximate result in Fig. 3. The major boundaries and associated shear velocity contrasts are readily identified in both cases. Note that there is a slight 'pull-up' of underthrust material as a result of inadequacies in the 1-D reference model. Localization of structure

in the Kirchhoff inversion may be regarded as slightly better than the Born-approximate result which identifies the $\Delta\beta/\beta$ contrast as a perturbation to the reference model as opposed to a discontinuity surface whose amplitude is proportional to the contrast.

7 CASC93

As a second demonstration of the Kirchhoff inversion we turn to the IRIS-PASSCAL data set recorded over central Oregon by researchers at the Oregon State University (Li 1996; Nabelek *et al.* 1993), (see also Rondenay *et al.* 2001). This experiment involved the deployment of some 40 seismometers at a total of 69 sites between May 1993 and March 1994. The sites were located along an east-west line extending from the coast across the Cascades well into the backarc region with an average of 5 km spacing. We have selected a subset of 31 events with high-signal-to-noise ratios as input to the Kirchhoff-approximate inversion (see Rondenay *et al.* 2001, for details on event selection etc.). For this event sampling, the backscattered *S*-response due to the free-surface *P*-reflection (i.e. mode $m = 4$) is strongest and thus we focus on the inversion results for this mode alone.

Fig. 4 shows the results for both Born (see Rondenay *et al.* 2001) and Kirchhoff inversions of this data set. Two prominent structures appear within the Born result. The continental Moho is evident as a change from negative to positive shear velocity perturbation near 40 km depth, which extends from 150 km to the eastern end of the model at 240 km. The western portion of the model is dominated by the response of the subducting Juan de Fuca plate. At shallower levels, the oceanic crust is evident as a low-velocity, 10 km thick layer, dipping gently at 16 degrees and sandwiched between higher velocity material (mantle below and the Siletz terrane above). Near 30 km depth there is a disruption in this pattern as the top of the oceanic crust appears to deflect horizontally for a few 10's of km and the intensity of its signature diminishes. A weaker oceanic Moho continues to depths of at least 100 km with a dip of approximately 30 degrees. This response is interpreted to manifest the effects of dehydration/eclogitization in the downgoing oceanic crust and rehydration/mineral precipitation in the wedge above. Most of the aforementioned structures are also evident in the Kirchhoff result, though they are rather less well resolved. The cause of the poorer reconstruction originates in the different frequency filters that are used to preprocess data for the two algorithms. Because of the effects of unmodelled scattering (e.g. surface-wave scattering from topography, 3-D scattering) and noise, the lower frequencies in the wavefield exhibit greater coherence than the high frequencies. The preferential weighting given to the (less-coherent) higher frequencies in the Kirchhoff approach thus leads to the poorer image.

8 CONCLUSIONS

We have developed a 2-D Kirchhoff-approximate inversion method for teleseismic waves that permits retrieval of isotropic, material property contrasts across crust and mantle discontinuities. The development relies on a form of Kirchhoff-Helmholtz integral involving wave modes (versus the more traditional formulation in terms of traction and displacement), and the analogy of the high-frequency scattering equations with the generalized Radon transform (Beylkin 1985). Although developed for teleseismic wavefields and 2-D structures, the approach is easily generalized to other source configurations and 3-D structures. In particular, it extends the Kirchhoff-approximate treatment of Beylkin & Burridge (1990) involving *P*-to-*P* interactions, to *S*-waves and conversions.

We have compared the Kirchhoff-approximate inversion to a related method employing the Born approximation in applications to both synthetic and field data sets. Results for the synthetic data set indicate a better localization of stratification using the Kirchhoff inversion, which suggests that it should be preferred in applications to field data. However, field data suffer from contamination by incoherent and unmodelled scattering which becomes more pronounced at higher frequencies. The Kirchhoff approximation requires that data be preprocessed with a high-pass filter thereby amplifying this contamination. The result is a rather poorer recovery of subduction zone structure when applied to data from the CASC93 experiment. Mitigation of the effects of unmodelled scattering from teleseismic waveform inversion is the topic of ongoing research.

REFERENCES

Aki, K. & Richards, P.G., 1980. *Quantitative Seismology—Theory and Methods,* Vol. 1, W.H. Freeman, San Fransisco.

Beylkin, G., 1985. Imaging of discontinuities in the inverse scattering problem by inversion of a causal generalized Radon transform, *J. Math. Phys.,* **26,** 99–108.

Beylkin, G. & Burridge, R., 1990. Linearized inverse scattering problems in acoustics and elasticity, *Wave Motion,* **12,** 15–52.

Bleistein, N., 1987. On the imaging of reflectors in the earth, *Geophysics,* **52,** 931–942.

Bostock, M.G., Rondenay, S. & Shragge, J., 2001. Multi-parameter 2-D inversion of scattered teleseismic body-waves—I. Theory for oblique incidence, *J. geophys. Res.,* **160,** 30 771–30 782.

Docherty, P., 1991. A brief comparison of some Kirchhoff integral formulas for migration and inversion, *Geophysics,* **56,** 1164–1169.

Dueker, K.G. & Sheehan, A.F., 1997. Mantle discontinuity structure from midpoint stacks of converted P to S waves across the Yellowstone hotspot track, *J. geophys. Res.,* **102,** 8313–8327.

Frazer, L.N. & Sen, M.K., 1985. Kirchhoff-Helmholtz reflection seismograms in a laterally inhomogeneous multi-layered elastic medium—I. Theory, *Geophys. J. R. astr. Soc.,* **80,** 121–147.

Kuo, J.T. & Dai, T.-F., 1984. Kirchhoff elastic wave migration for the case of noncoincident source and receiver, *Geophysics,* **49,** 1223–1238.

Langston, C.A., 1979. Structure under Mount Rainier, Washington, inferred from teleseismic body waves, *J. geophys. Res.,* **84,** 4749–4762.

Li, X.-Q., 1996. Deconvolving orbital surface waves for the source duration of large earthquakes and modeling the receiver functions for the earth structure beneath a broadband seismometer array in the Cascadia subduction zone, *PhD thesis,* p. 153, Oregon State Univ., Corvallis, September.

Miller, D., Oristaglio, M. & Beylkin, G., 1987. A new slant on seismic imaging: Migration and integral geometry, *Geophysics,* **52,** 943–964.

Morse, P.M. & Feshbach, H., 1953. *Methods of Theoretical Physics,* McGraw-Hill, New York.

Nabelek, J., Li, X.-Q., Azevedo, S., Braunmiller, J., Fabritius, A., Leitner, B., Tréhu, A.M. & Zandt, G., 1993. A high-resolution image of the Cascadia subduction zone from teleseismic converted phases recorded by a broadb and seismic array, *EOS, Trans. Am. geophys. Un., 74 (43, fall meeting suppl.),* 431.

Pao, Y.-H. & Varatharajulu, V., 1976. Huygens' principle, radiation conditions and integral formulas for the scattering of elastic waves, *J. acoust. Soc. Am.,* **59,** 1361–1371.

Revenaugh, J., 1995. A scattered-wave image of subduction beneath the Transverse Ranges, *Science,* **268,** 1888–1892.

Rondenay, S., Bostock, M.G. & Shragge, J., 2001. Multi-parameter 2-D inversion of scattered teleseismic body-waves—III. Application to CASC93, *J. geophys. Res.,* **106,** 30 795–30 807.

Ryberg, T. & Weber, M., 2000. Receiver function arrays: a reflection seismic approach, *Geophys. J. Int.,* **141,** 1–11.

Schneider, W.A., 1978. Integral formulation for migration in two and three dimensions, *Geophysics,* **43,** 49–76.

Shearer, P.M., Flanagan, M.P. & Hedlin, M.A.H., 1999. Experiments in migration processing of *SS* precursor data to image upper mantle discontinuity structure, *J. geophys. Res.,* **104,** 7229–7242.

Shragge, J., Rondenay, S. & Bostock, M.G., 2001. Multi-parameter 2-D inversion of scattered teleseismic body-waves—II. Numerical examples, *J. geophys. Res.,* **106,** 30 783–30 793.

Sumner, B., 1987. Kirchhoff-Helmholtz representations for scattered elastic fields, *Consortium Project on Seismic Inverse Methods for Complex Structures, Report 060,* Center for Wave Phenomena, Colorado School of Mines, Golden Colorado.

Vinnik, L.P., 1977. Detection of waves converted from *P* to *SV* in the mantle, *Phys. Earth planet. Inter.,* **15,** 39–45.

Waterman, P.C., 1978. Matrix theory of elastic wave scattering—II. A new conservation law, *J. acoust. Soc. Am.,* **63,** 1320–1325.

APPENDIX A: LINEARIZED R/T COEFFICIENTS

The linearized R/T coefficients of Aki & Richards (1980) are written in the notation of this study as:

$$R_D^{PP} = \frac{1}{2\cos^2\tilde\theta^P}\frac{\Delta\alpha}{\alpha} - 4\left(\frac{\beta}{\alpha}\right)^2 \sin^2\tilde\theta^P \frac{\Delta\beta}{\beta}$$
$$+ \frac{\alpha^2 - 4\beta^2\sin^2\tilde\theta^P}{2\alpha^2}\frac{\Delta\rho}{\rho}, \tag{A1}$$

$$R_D^{PS} = \left(\frac{2\sin^3\tilde\theta^S}{\cos\hat\theta^P} - \frac{\beta}{\alpha}\sin 2\tilde\theta^S\right)\frac{\Delta\beta}{\beta}$$
$$- \left(\frac{\sin\tilde\theta^S \cos 2\tilde\theta^S}{2\cos\hat\theta^P} + \frac{\beta\sin 2\tilde\theta^S}{2\alpha}\right)\frac{\Delta\rho}{\rho}, \tag{A2}$$

$$R_D^{VV} = -\frac{\cos 4\tilde\theta^S}{2\cos^2\tilde\theta^S}\frac{\Delta\beta}{\beta} - \frac{1}{2}(1 - 4\sin^2\tilde\theta^S)\frac{\Delta\rho}{\rho}, \tag{A3}$$

$$R_D^{SP} = \left(\frac{2\sin\tilde\theta^P \sin^2\hat\theta^S}{\cos\hat\theta^S} - \frac{\beta}{\alpha}\sin 2\tilde\theta^P\right)\frac{\Delta\beta}{\beta}$$
$$- \left(\frac{\sin\tilde\theta^P \cos 2\hat\theta^S}{2\cos\hat\theta^S} + \frac{\beta\sin 2\tilde\theta^P}{2\alpha}\right)\frac{\Delta\rho}{\rho}, \tag{A4}$$

$$R_D^{HH} = \left(1 - \frac{1}{2\cos^2\tilde\theta^S}\right)\frac{\Delta\beta}{\beta} + \frac{1}{2}\frac{\Delta\rho}{\rho}, \tag{A5}$$

$$T_U^{PS} = R_D^{PS}$$
$$T_U^{SP} = R_D^{SP}, \tag{A7}$$

The angular quantities (see Fig. 2) are defined through

$$\cos\tilde\theta = \tilde c\frac{\nabla\tilde\tau \cdot \nabla\mathcal{T}^m}{|\nabla\mathcal{T}^m|}, \quad \cos\hat\theta = \hat c\frac{\nabla\hat\tau \cdot \nabla\mathcal{T}^m}{|\nabla\mathcal{T}^m|}, \tag{A8}$$

which implies $\theta = \tilde\theta + \hat\theta$ in general, and $\hat\theta = \tilde\theta$ for intramode reflections. This definition of angles leads to expressions for the upward transmission-conversion coefficients T_U^{PS}, T_U^{SP}, that are identical to their topside reflection-conversion counterparts R_D^{PS}, R_D^{SP}, except that they are employed over different ranges of scattering angle θ. The linearized reflection coefficients are valid for θ close to 0° whereas the expressions for transmission coefficients are valid for θ near 180°. Accordingly, the summation in (23) should be limited to traces corresponding to scattering angles of less than some maximum angle, say 45° about $\theta = 0°$ (reflections), or $\theta = 180°$ (transmissions). Note, however, that in general, the linearized approximations are stable for angles approaching critical although often inaccurate. The exceptions are R_D^{PS}, T_U^{PS} which exhibit singular behaviour as $\tilde\theta^P$ approaches 90°, a characteristic not shared by the corresponding, exact expressions.